DOI: 10.1002/anie.201100181

Protein–Mineral Interactions

Single-Molecule Determination of the Face-Specific Adsorption of Amelogenin's C-Terminus on Hydroxyapatite**

Raymond W. Friddle, Keith Battle, Vasily Trubetskoy, Jinhui Tao, E. Alan Salter, Janet Moradian-Oldak, James J. De Yoreo, and Andrzej Wierzbicki**

The energetics of protein–mineral interactions is a crucial but poorly characterized factor underlying the hierarchical structure of mineralized tissue. During mineralization, organized protein matrices direct formation of mineral components. As with all assembly processes, the free-energy change provides the underlying thermodynamic driver, in this case reflecting protein interactions with the nascent mineral. However, despite the importance of obtaining face-specific free energies of mineral binding to establish a molecular-level understanding of biomineral organization, to date no direct measurements have been reported. Computational approaches struggle with the complexities of proteins, the inadequacies of model water potentials and effects of background electrolytes. Herein we present a novel application of force spectroscopy in which an atomic force microscopy (AFM) tip, functionalized with Amelogenin protein (Amel) C-terminal fragment, is used to directly determine the single-molecule, face-specific free energy ΔG_B of Amel binding to hydroxyapatite (HAp), the mineral phase in tooth enamel.[1] We then use complementary molecular dynamics (MD) simulations to compare binding energies at different faces and surface terminations and to identify the key interactions controlling face-specific binding and crystal morphology.

Amelogenin (Table 1), a largely hydrophobic protein rich in proline, self-assembles to form oblate nanoparticles[2] comprised of approximately 100 monomers.[3,4] Recent in-vitro crystallization experiments show that Amel stabilizes calcium phosphate (Ca-P) clusters, which assemble as composite Amel-Ca-P nanoclusters.[5] These clusters co-assemble as chains of nanoparticles that evolve into long co-aligned crystals resembling those found in biological enamel.[5] Crystal-growth experiments,[6,7] NMR spectroscopy studies,[8–10] and neutron scattering[11] demonstrate a specific interaction between Amel and HAp crystal faces, with the Amel C-terminal region implicated as essential, and with the latter two techniques providing direct evidence that the C-terminus is close enough to the HAp surface to direct growth. Amel-assisted HAp formation leads to expression of elongated prismatic (100) crystals with the basal (001) faces defining the enamel/saliva interface.[12] This crystal habit differs from that of uninhibited, inorganically grown HAp, which exhibits short, prismatic (100) or stubby (001) morphologies,[13] or HAp crystals grown during bone formation, which are thin plates elongated along the c-axis.[14,15] Thus, it is suspected that Amel binds to the (100) face, thereby inhibiting HAp growth along (100) and inducing c-axis elongation.[16]

Solid-state NMR spectroscopy studies of LRAP, which is both a naturally occurring splice variant of Amel with preserved N- and C-termini (Table 1) and an inhibitor of HAp growth,[17] have established that the last approximately 18 residues of LRAP's C-terminal region lie flat on the HAp surface with significant mobility and without three-dimensional folding.[8–10] LRAP's role in enamel development has not been established, but promotion of enamel growth has been proposed.[18] MD studies, which have also provided some insights into the geometry of Amel-HAP binding,[19] can in principle delineate the energetics of binding. However, while NMR data provide a good experimental constraint on the structural aspects of simulations, no such constraints on energetics are available. Assays based on inhibition of growth are indirect and qualitative. Experimental approaches that quantitatively probe interaction free energies are typically based on bulk measurements that average over all faces, edges and corners, and the free energies obtained are relative to standard state conditions. These are difficult to relate to computations of face-specific binding free energies for a single-molecule.

Single-molecule force spectroscopy can circumvent both problems by providing a clear definition of states at the molecular level and allowing direct control over the location of interaction. To this end, we functionalized the tip of an AFM cantilever with the 13-mer terminal fragment of Amel (Table 1) and collected force–distance curves associated with binding to the (100) HAp face (Figure 1a). The peptide was

[*] Dr. R. W. Friddle, V. Trubetskoy, Dr. J. Tao, Dr. J. J. De Yoreo
Molecular Foundry, Lawrence Berkeley National Laboratory
Berkeley, CA 94720 (USA)
E-mail: jjdeyoreo@lbl.gov
K. Battle, Dr. E. A. Salter, Prof. A. Wierzbicki
Department of Chemistry, University of South Alabama
Mobile, AL 36688 (USA)
E-mail: awierzbi@jaguar1.usouthal.edu
Prof. J. Moradian-Oldak
Center for Craniofacial Molecular Biology
University of Southern California
Ostrow School of Dentistry, Los Angeles, CA 90033 (USA)

[**] This work was supported by NIH grant DE003223 and made possible in part by a grant of high-performance computing resources and technical support from the Alabama Supercomputing Authority. Force spectroscopy method development was supported by the Office of Science, Office of Basic Energy Sciences of the U.S. Department of Energy under Contract no. DE-AC52-07NA27344. Measurements were performed at the Molecular Foundry, Lawrence Berkeley National Laboratory with support from the Office of Science, Office of Basic Energy Sciences of the U.S. Department of Energy under Contract no. DE-AC02-05CH1123.

Supporting information for this article is available on the WWW under http://dx.doi.org/10.1002/anie.201100181.

Table 1: Sequences of Amelogenin, LRAP, and C-terminal 13-mer.[a]

Amelogenin	PLPPHPGHPG YINFSYEVLT PLKWYQNMIR HPYTSYGYEP MGGWLHHQII PVVSQQTPQS HALQPHHHIP MVPAQQPGIP QQPMMPLPGQ HSMTPTQHHQ PNLPLPAQQP FQPQPVQPQP HQPLQPQSPM HPIQPLLPQP PLPPMFSMQS LLPDLPLEAW PATDKTKREE VD
LRAP	PLPPHPGHPG YINFSYEVLT PLKWYQNMIR HPSLLPDLPL EAWPATDKTK REEVD
13-mer[b]	W PATDKTKREE VD

[a] Porcine.[35,36] The splice variant LRAP sequence is indicated in blue and red. [b] Note that the MD simulations were performed using the 12-mer which is identical to the 13-mer with the removal of the W at the N-terminus.

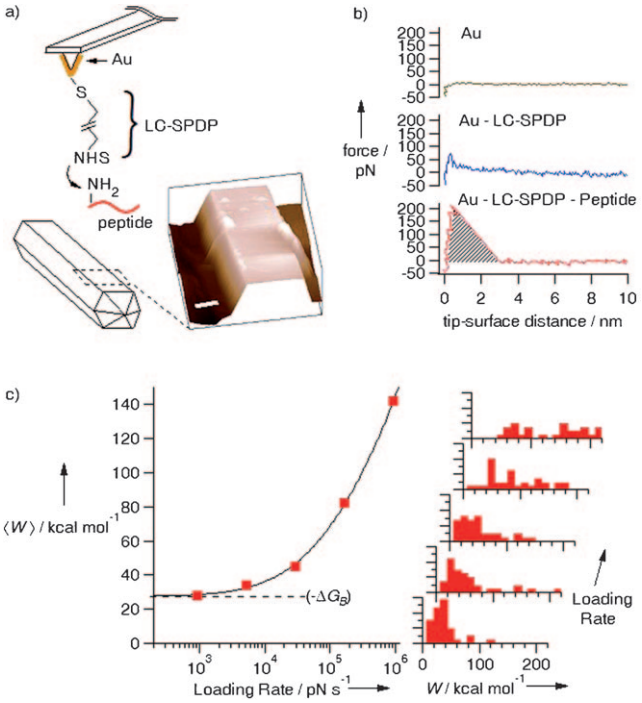

Figure 1. Determination of the free energy of binding of the C-terminal sequence of Amelogenin adsorbed to the (100) face of HAp. a) The peptide is linked to a gold-coated AFM cantilever by way of a bifunctional linker. The tip is placed directly on the (100) face of individual HAp crystals, which were visible under bright-field optics. Inset: typical AFM scan of an HAp crystal used to characterize the surface before force measurements (scale bar 4 μm). b) Representative force–distance curves for each level of functionalization (Au coating, LC-SPDP linker, and peptide) at approximately equivalent loading rates (4.7, 3.6, and 5.3 nN s^{-1}, respectively). The hatched region indicates the work, *W*, measured upon moving the cantilever tip from the surface to the minimum of the pulling potential. c) Means (solid squares) and corresponding histograms (solid bars) of work measured from repeated force–distance trajectories for a peptide-functionalized tip (spring constant 93 pN nm^{-1}) from the (100) face of HAp. Solid curve is a fit to a two-state theoretical model given in the Supporting Information. The mean work tends asymptotically to a finite value given by the free-energy difference (dashed line) of $\Delta G_B = -27.6$ kcal mol^{-1}. The normalized histograms for increasing loading rate (0.93, 5.25, 29.5, 165.9, and 933 nN s^{-1}) are offset for clarity using identical ranges along the two axes.

linked to gold-coated Si_3N_4 AFM tips through a heterobifunctional cross-linker LC-SPDP (Thermo Scientific) consisting of a pyridyl disulfide, which adsorbed to the Au, and an *N*-hydroxysuccinimide (NHS) ester that reacted with the N-terminal amine or lysine residues of the peptide to form an amide bond. (See Section S2 of the Supporting Information for details.) Deprotonated primary amines (such as Lys and N-terminus) react with NHS ester through nucleophilic attack to form a stable covalent bond. Hydrolysis of the NHS ester competes with this reaction, and the rate of hydrolysis increases with increasing pH value. Therefore we performed peptide linking to the NHS ester-bearing tips in phosphate buffered saline solution (PBS; Sigma Aldrich) at pH 7.4. This pH value facilitated a preference for linking to the N-terminal amine, which had a greater probability of existing in the deprotonated form, owing to a pK_a value much lower than the pK_a of the Lys residues (ca. 10.5). In addition, a limited concentration of peptide was used to functionalize tips in order to optimize the chances of linking a single molecule at the tip. As a result, several prepared tips gave little to no interaction with the crystal face, consistent with the control tips, which also gave very little interaction (Figure 1b, two top curves). Figure 1b shows representative force–distance trajectories for each level of chemical functionalization. We found independent measurements with peptide-functionalized tips gave strong, consistent interaction forces. Figure 1b, bottom curve, shows data for one of these experiments. (Between 40 and 100 individual force curves were collected and analyzed for each data point. For further data, see Figure S1, Supporting Information.)

The force–distance curves can be converted directly into the work *W* associated with breaking the Amel–HAp bond by integrating over the shaded area in Figure 1b. Because the bond rupture process is time-dependent, this work is greater than the equilibrium free energy of binding ΔG_B by an amount of dissipated heat, which decreases with decreasing loading rate d*F*/d*t*. As d*F*/d*t* approaches zero, the rate of bond breaking approaches its equilibrium value and the work done on the system should approach ΔG_B. Figure 1c shows the mean work $\langle W \rangle$ versus d*F*/d*t* and the corresponding normalized frequency histograms for each loading rate. As expected, $\langle W \rangle$ falls with decreasing loading rate and extrapolates to a finite value at d*F*/d*t* = 0.

The solid curve in Figure 1c is a fit to the data according to a theoretical model that accounts for the kinetics of forced desorption from the adsorbed state (see Section S5 of the Supporting Information for details). The model predicts two major regimes with loading rate: a non-linear regime at large loading rates, characterized primarily by the kinetics of forced desorption, and a linear regime at small loading rates where the desorption and adsorption rates are comparable. The linear regime appears as a plateau in the plot of $\langle W \rangle$ versus log(d*F*/d*t*) and tends asymptotically to the equilibrium free-energy difference between the adsorbed and desorbed states. The fit to the data is excellent, and the asymptote gives $\Delta G_B = -27.6 \pm 1.5$ kcal mol^{-1}. Data for a second peptide-functional-

ized tip (Figure S1, Supporting Information) yields $\Delta G_B = -29.5 \pm 1.3$ kcal mol^{-1}, giving an average value of $\langle \Delta G_B \rangle = -28.6 \pm 1.4$ kcal mol^{-1}, a value larger than but comparable to the -7 to -10 and -18.3 kcal mol^{-1} calorimetric values reported for the statherin/HAp[20] and biotin/streptadivin[21] systems, respectively.

These measurements were complemented by molecular dynamics (MD) adaptive biasing force (ABF) simulations in which the same Amel fragment (minus the N-terminal tryptophan) was gradually lifted from the HAp surface to obtain potential of mean force (PMF) adsorption free energies. Unlike the experiments, in which the elongated habit of the HAp crystals prevented direct measurement of ΔG_B on the (001) face, the simulations enabled a direct comparison between binding to the (100) and (001) faces.

Figure 2 shows the computational models for various (100) and (001) surface terminations. Figure 3 shows the PMF free-energy profiles for lifting the 12-mer from these surfaces. The results predict the 12-mer binds more strongly to (100) than to (001) surfaces for both explicit and implicit water models (see also Table S1 of Supporting Information), and the preference is significant. For reference, a difference in binding energies greater than 4 kcal mol^{-1} implies a preference of over 1000:1 at room temperature. The 12-mer binds most strongly to termination 2 of the (100) surface indicated in Figure 2, in which the uppermost layer of calcium ions are stripped away. Moreover, this surface gives the best agreement between simulation distances and NMR data, Table 2, with a root mean squared (RMS) error of 1.1 Å for the peptide-to-surface distances. Distance measurements for binding orientations on all other flat surfaces give significantly poorer results (see Table S2 in Supporting Information) with RMS errors over 3.4 Å. Thus, the simulations provide a plausible model for the LRAP terminal fragment bound to the (100)-2 surface. (See Figure S3 of Supporting Information for detailed geometry). In addition, while there is

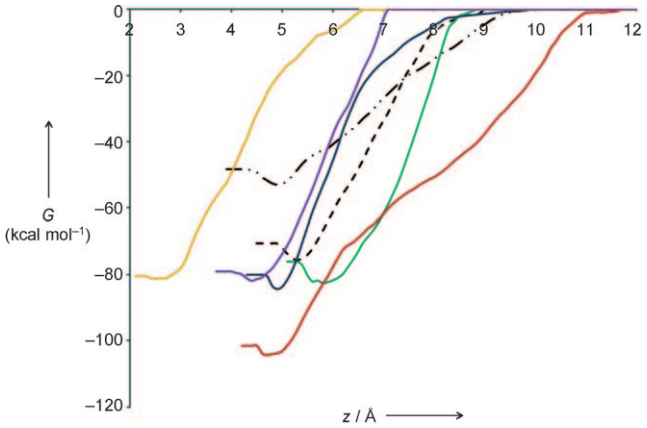

Figure 3. Adsorption free-energy PMFs from ABF simulations for 12-mer/HAp systems. Potentials are derived from several independent 500 ps simulations in which the center of the biasing potential of the 12-mer was "pulled" along the *z*-axis, normal to the HAp surfaces. The 12-mer binds more favorably to the various terminations (see Figure 2) of the (100) surface than to the (001) surfaces. Solid lines: (100)-1 (green), (100)-2 (red), (100)-3 (blue), (100)-4A (gold), (100)-4B (purple). Dashed black line: (001)-1; dot-dashed black line: (001)-2.

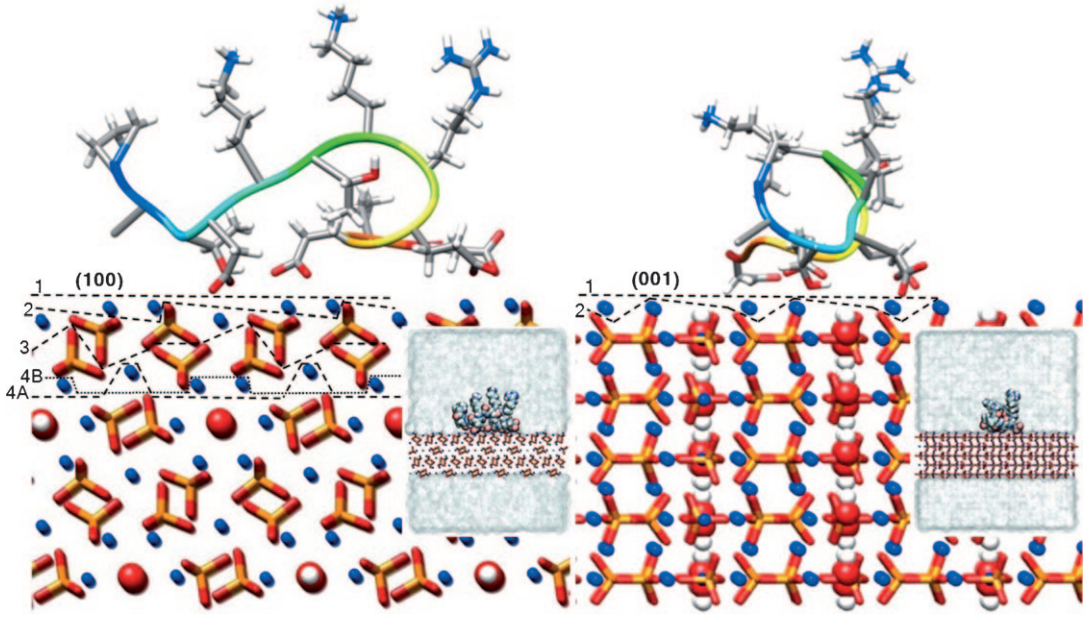

Figure 2. Initial orientations of the 12-mer on the calcium-terminated (100)-1 (left) and (001)-1 (right) HAp surfaces. Calcium ions are depicted in blue (ball), hydroxide ions in red and white (CPK), and phosphates in red/orange (tube). The 12-mer backbone is depicted in rainbow as a tube, with blue representing the N-terminus (P-1) and red representing the C-terminus (D-12); selected nonpolar hydrogen atoms are hidden from view. Five carboxylate moieties of the 12-mer account for the strong ionic attraction to the Ca^{2+}-terminated surfaces. Other (100) surface terminations 2, 3, 4A, and 4B, and an alternate (001) termination 2 are indicated (as dashed black lines). The hydroxide ions in the HAp lattice are emphasized as CPK models to highlight the random orientations of the hydroxide columns. Insets: The solvated systems under periodic boundary conditions are shown, with water molecules represented as transparent isosurfaces.

Table 2: Selected simulation distances [Å] for the adsorbed 12-mer on the (100)-2 HAp Surface.[a]

Distance	(100)-2	Exp.[b]
A-49 (C^{α}) to surface P (A-2)	5.3 ± 0.1	– 6.0 ± 0.5
K-52 (N^{ζ}) to surface P (K-5)	3.5 ± 0.1	4.0 ± 1.0 5.8 ± 0.5
K-54 (C′) to surface P (K-7)	5.0 ± 0.2	6.5 ± 0.5 6.0 ± 0.5
V-58 (N) to surface P (V-11)	4.3 ± 0.1	– 5.8 ± 0.5
V-58 (C′) to surface P (V-11)	4.8 ± 0.1	5.8 ± 0.5 5.4 ± 0.5
A-49 (C′) to T-53 (N) (A-2) (T-6)	10.7 ± 0.1	6.9 ± 1.0 6.1 ± 0.5
K-54 (C′) to V-58 (N) (K-7) (V-11)	5.5 ± 0.4	5.5 5.5

[a] Computational values are averages obtained over post-equilibration periods of 500 ps. C′ denotes carbonyl carbon atom; N denotes backbone nitrogen atom. Distances are defined using LRAP residue numbering, with corresponding 12-mer numbering in parentheses. [b] Solid-state NMR spectroscopic data for LRAP on indeterminate HAp surface.[8,10] Values for bound, hydrated sample are given as first entries; values for bound, lyophilized sample are given second.

no way of knowing a priori which termination of the (100) surface is expressed, the fact that the (100)-2 surface termination gives both the best agreement with the NMR data and the largest free energy of adsorption lends credence to this being the most likely termination for the HAp (100) surface.

As an alternative scenario, we performed simulations of 12-mer binding to a stepped calcium-terminated (100)-1 surface (Figure S4 of Supporting Information). This model likewise appears plausible, because there is also good agreement with NMR data with an RMS error of 0.7 Å. However, because our AFM analysis shows the step density is only about one per 100 nm on the (100) surface, we have not pursued this alternative further.

Not surprisingly, the range of computed binding energies for the (100) surfaces in explicit water (−83 to −104 kcal mol^{-1}) is greater in magnitude than the experimental result, while the estimates of −6 to −15 kcal mol^{-1} for implicit water ($\varepsilon = 80$) are relatively low (see Table S2 of the Supporting Information). Generally, interaction energies of charged organic species on surfaces of ionic crystals are overestimated in explicit water simulations due to a mismatch of force-field charge assignments between the organic and mineral components.[22,23] The standard protocol for explicit water calculations calls for unscaled Coulombic interactions ($\varepsilon = 1$), yet long-range dielectric screening by an unpolarizable solvent model is underestimated.[24] On the other hand, implicit water (homogeneous dielectric environment, $\varepsilon = 80$) quenches the normally solvent-inaccessible short-range interactions which dominate the binding energy. From inspection of both sets of binding energies for the (100) surfaces, we see the simulation results preserve the order of binding affinities and bracket the experimental result. In fact, when we compute PMFs using an intermediate dielectric constant with the explicit water model, we find that the binding energies are scaled by a nearly constant factor and the preference for the (100)-2 surface over both (001) surfaces is maintained.

Previous studies[2,5,25] have concluded that the self-assembled amelogenin nanospheres present their hydrophilic C-termini toward the exterior, away from the primarily hydrophobic cores.[26] C-terminus interactions should therefore dominate Amel-HAp binding. Thus, our finding that binding to (100) is strongly preferred over binding to (001) is consistent with the hypothesis that Amel-assisted HAp formation achieves elongation along (001) by selectively inhibiting (100) growth.

Because single-molecule force spectroscopy is the only direct experimental analogue to MD simulations of molecular binding, this work establishes a link between experiment and computation through the determination of the Amel free energy of binding to specific faces of HAp. Our results show the binding free energy is comparable to that of other strong biomolecular interactions, such as biotin-to-streptadivin and statherin-to-HAp. This strong interaction comes about because the carboxylic groups of the C-terminus bind preferentially to the calcium ions of the (100) surface in a manner similar to that predicted for LRAP bound to (001).[19] However, our simulations provide a structural and energetic rationale for predicting that the (100) face is the relevant surface for Amel binding. Moreover, from inspection of the 12-mer to the (100)-2 surface binding scenario, we conclude that positively charged C-terminus residues may also play an important role in binding, as was also suggested for statherin.[20] Finally, our combined computational and experimental findings link the atomic-level interactions of Amel with specific faces of HAp to the experimentally observed growth habit of HAp.

Experimental Section

Details of tip functionalization are found in the Supporting Information. In brief, microlever Si_3N_4 AFM tips (Veeco, Plainview, NY) were coated with gold by thermal evaporation, and then immersed in a DMF solution containing 0.2 mM of the heterobifunctional cross-linker LC-SPDP (Thermo Scientific), which bears a pyridyl disulfide that binds to gold, leaving a low density of *N*-hydroxysuccinimide (NHS) ester groups presented at the tip surface. After removing unbound cross-linker, the ester-modified tips were immersed in a peptide solution (0.2 mM in PBS) to form a stable amide bond with a primary lysine residue or terminal amine of the peptide. Force measurements between modified tips and HAp crystals were performed under calcium phosphate solution at approximately equilibrium saturation with the crystal. Measurements were made with the MFP3D Atomic Force Microscope (Asylum Research, Santa Barbara, CA). To account for any surface heterogeneity, a custom routine randomly sampled points on the surface to give a representative average. A constant approach velocity of 200 nm s^{-1} was used for every pulling speed studied. A 2–3 nm deflection trigger was used to contact the surface and dwell for 1 second before pulling away.

Details of the simulations are given in the Supporting Information. Briefly, Cerius[2] software[27] was used to create slabs of HAp, which has alternating positively and negatively charged layers. Apparent cleavage planes shown in Figure 2 define the positively charged calcium-terminated (100)-1 and (001)-1 surfaces. Because the actual HAp surface terminations are unknown, some other terminations of the (100) and (001) surfaces were modeled as indicated in Figure 2. We assigned the CHARMM22 force-field parameter set[28] to the 12-mer and incorporated the nonbonding parameters and atom charges for HAp[29,30] to set up fixed-lattice simulations of the HAp/12-mer system using NAMD 2.7.[31] The peptide's starting configuration was an equilibrated solution-state structure (1 ns in TIP3P water), and after preliminary docking to the HAp surface, NVT adaptive biasing force (ABF) simulations[32–34] (500 ps) were carried out in TIP3P water and in the gas phase ($\varepsilon = 80$) using periodic boundary conditions. Selected distances were averaged over the last 500 ps of a 4 ns simulation for comparisons with solid-state NMR spectroscopy data.

Received: January 10, 2011
Revised: April 15, 2011
Published online: June 27, 2011

Keywords: adsorption free energy · amelogenin · force spectroscopy · hydroxyapatite · molecular dynamics

[1] H. C. Margolis, E. Beniash, C. E. Fowler, *J. Dent. Res.* **2006**, *85*, 775.
[2] B. Aichmayer, F. B. Wiedemann-Bidlack, C. Gilow, J. P. Simmer, Y. Yamakoshi, F. Emmerling, H. C. Margolis, P. Fratzl, *Biomacromolecules* **2010**, *11*, 369.
[3] A. G. Fincham, J. Moradian-Oldak, J. P. Simmer, P. Sarte, E. C. Lau, T. Diekwisch, H. C. Slavkin, *J. Struct. Biol.* **1994**, *112*, 103.
[4] J. Moradian-Oldak, J. P. Simmer, E. C. Lau, P. E. Sarte, H. C. Slavkin, A. G. Fincham, *Biopolymers* **1994**, *34*, 1339.
[5] X. Yang, L. Wang, Y. Qin, Z. Sun, Z. J. Henneman, J. Moradian-Oldak, G. H. Nancollas, *J. Phys. Chem. B* **2010**, *114*, 2293.
[6] T. Aoba, M. Fukae, T. Tanabe, M. Shimizu, E. C. Moreno, *Calcif. Tissue Int.* **1987**, *41*, 281.
[7] J. Moradian-Oldak, N. Bouropoulos, L. Wang, N. Gharakhanian, *Matrix Biol.* **2002**, *21*, 197.
[8] W. J. Shaw, A. A. Campbell, M. L. Paine, M. L. Snead, *J. Biol. Chem.* **2004**, *279*, 40263.
[9] W. J. Shaw, K. Ferris, *J. Phys. Chem. B* **2008**, *112*, 16975.
[10] W. J. Shaw, K. Ferris, B. Tarasevich, J. L. Larson, *Biophys. J.* **2008**, *94*, 3247.
[11] W. J. Shaw, K. F. Ferris, S. Krueger, U. Perez-Salas, V. Silin, D. J. McGillivray, A. A. Campbell, M. L. Paine, M. L. Snead in *Eighth International Conference on the Chemistry and Biology of Mineralized Tissues*, **2004**, p. 150.
[12] R. J. Radlanski, W. Seidl, G. Steding, A. Jäger, *Anat. Anz.* **1989**, *168*, 405.
[13] C. Palache, H. Berman, C. Frondel, *The System of Mineralogy of James Dwight Dana and Edward Salisbury Dana*, *Vol. II*, 7 ed., Wiley, New York, **1951**.
[14] S. Weiner, H. D. Wagner, *Annu. Rev. Mater. Sci.* **1998**, *28*, 271.
[15] P. Fratzl, N. Fratzl-Zelman, K. Klaushofer, G. Vogl, K. Koller, *Calcif. Tissue Int.* **1991**, *48*, 407.
[16] M. L. Wallwork, J. Kirkham, J. Zhang, D. A. Smith, S. J. Brookes, R. C. Shore, S. R. Wood, O. Ryu, C. Robinson, *Langmuir* **2001**, *17*, 2508.
[17] J. Moradian-Oldak, J. Tan, A. G. Fincham, *Biopolymers* **1998**, *46*, 225.
[18] R. M. H. Ravindranath, A. Devarajan, P. Bringas, Jr., *Arch. Oral Biol.* **2007**, *52*, 1161.
[19] X. Chen, Q. Wang, J. Shen, H. Pan, T. Wu, *J. Phys. Chem. C* **2007**, *111*, 1284.
[20] R. Goobes, G. Goobes, C. T. Campbell, P. S. Stayton, *Biochemistry* **2006**, *45*, 5576.
[21] P. C. Weber, J. J. Wendoloski, M. W. Pantoliano, F. R. Salemme, *J. Am. Chem. Soc.* **1992**, *114*, 3197.
[22] D. M. Duffy, J. H. Harding, *Langmuir* **2004**, *20*, 7630.
[23] C. L. Freeman, J. H. Harding, D. J. Cooke, J. A. Elliott, J. S. Lardge, D. M. Duffy, *J. Phys. Chem. C* **2007**, *111*, 11943.
[24] I. V. Leontyev, A. A. Stuchebrukhov, *J. Chem. Theory Comput.* **2010**, *6*, 1498.
[25] L. C. Palmer, C. J. Newcomb, S. R. Kaltz, E. D. Spoerke, S. I. Stupp, *Chem. Rev.* **2008**, *108*, 4754.
[26] C. Du, G. Falini, S. Fermani, C. Abbott, J. Moradian-Oldak, *Science* **2005**, *307*, 1450.
[27] Cerius[2] 4.8.1, Accelrys, San Diego, CA, 2003.
[28] A. D. MacKerell, Jr., D. Bashford, M. Bellott, R. L. Dunbrack, Jr., J. D. Evanseck, M. J. Field, S. Fischer, J. Gao, H. Guo, S. Ha, D. Joseph-McCarthy, L. Kuchnir, K. Kuczera, F. T. K. Lau, C. Mattos, S. Michnick, T. Ngo, D. T. Nguyen, B. Prodhom, W. E. Reiher III, B. Roux, M. Schlenkrich, J. C. Smith, R. Stote, J. Straub, M. Watanabe, J. Wiórkiewicz-Kuczera, D. Yin, M. Karplus, *J. Phys. Chem. B* **1998**, *102*, 3586.
[29] S. Hauptmann, H. Dufner, J. Brickmann, S. M. Kast, R. S. Berry, *Phys. Chem. Chem. Phys.* **2003**, *5*, 635.
[30] R. Bhowmik, K. S. Katti, D. Katti, *Polymer* **2007**, *48*, 664.
[31] J. C. Phillips, R. Braun, W. Wang, J. Gumbart, E. Tajkhorshid, E. Villa, C. Chipot, R. D. Skeel, L. Kale, K. Schulten, *J. Comput. Chem.* **2005**, *26*, 1781.
[32] E. Darve, A. Pohorille, *J. Chem. Phys.* **2001**, *115*, 9169.
[33] E. Darve, D. Rodriguez-Gomez, A. Pohorille, *J. Chem. Phys.* **2008**, *128*, 144120.
[34] J. Hénin, G. Fiorin, C. Chipot, M. L. Klein, *J. Chem. Theory Comput.* **2010**, *6*, 35.
[35] A. G. Fincham, A. B. Belcourt, J. D. Termine, W. T. Butler, W. C. Cothran, *Biochem. J.* **1983**, *211*, 149.
[36] Y. Yamakoshi, T. Tanabe, M. Fukae, M. Shimizu, in *Tooth Enamel V* (Ed.: R. W. Fearnhead), Florence, Yokohama, **1989**, p. 314.

